Carpio, P.; Borrell Tomás, MA.; Salvador Moya, MD.; Gómez, A.; Martínez, E.; Sánchez, E. (2015). Microstructure and mechanical properties of plasma spraying coatings from YSZ feedstocks comprising nano- and submicron-sized particles. Ceramics International. 41(3, Part A):4108-4117. doi:10.1016/j.ceramint.2014.11.106.

Microstructure and mechanical properties of plasma spraying coatings from YSZ feedstocks comprising nano- and submicron-sized particles

Pablo Carpio[1,*], Amparo Borrell[2], María Dolores Salvador[2], Andrés Gómez[3], Eduardo Martínez[3], Enrique Sánchez[1]

(1) Instituto de Tecnología Cerámica (ITC), Universitat Jaume I (UJI). Castellón, Spain

(2) Instituto de Tecnología de Materiales (ITM), Universitat Politècnica de València (UPV). Valencia, Spain

(3) Institut de Ciència dels Materials, Parc Cientific, Universitat de València, Valencia, Spain

Pablo Carpio (*corresponding author)

Telephone number: +34 964 342424 Fax number: +34 964 342425

Email: pablo.carpio@itc.uji.es

Postal address: Instituto de Tecnología Cerámica (ITC). Campus Universitario Riu Sec.

Av. Vicent Sos Baynat s/n

12006 Castellón (Spain)

Abstract

Atmospheric plasma spraying (APS) is an attractive technique to obtain nanostructured coatings due to its versatility, simplicity and relatively low cost. However, nanoparticles can not be fed into the plasma using conventional feeding systems, due to their low mass and poor flowability, and must be adequately reconstituted into sprayable micrometric agglomerates.

In this work, nanostructured and submicron-nanostructured powders of yttria-stabilised zirconia (YSZ) were deposited using APS, with a view to obtaining high-performance thermal barrier coatings (TBC). All powders were reconstituted by spray-drying from different solid loading suspensions, followed by a thermal treatment of the spray-dried granules to reduce agglomerate porosity and enhance powder sinterability. The reconstituted granules were characterised by XRD, SEM, pore sizing and flowability evaluation.

The reconstituted feedstocks were successfully deposited onto metallic substrates by APS. A metallic bond coat was sprayed between the substrate and the ceramic layer. The coating microstructure, characterised by SEM, was formed by partially melted zones, which retained the initial powder microstructure, embedded in a fully melted matrix which acts as a binder. It was shown that feedstock characteristics which in turn are very dependent of starting suspension characteristics, in particular agglomerate density and primary particle size, impact on coating microstructure (porosity and amount of partially-melted areas). For this reason mechanical properties of coatings are also strongly affected by feeding powder characteristics.

Key words: YSZ coatings; atmospheric plasma spraying; reconstituted powders; thermal barrier coatings

Introduction

Thermal barrier coatings (TBC) protect metallic substrates against exhaustive hot gases. Nowadays these materials are widely studied owing to their application on aeronautical or power technologies [1]. A top ceramic layer with thermal insulation properties and a metallic bond coat form these coatings. The bond coat usually comprises a MCrAlY (M = Ni and/or Co) alloy which develops two main functions: reducing the thermal contraction mismatch between the ceramic layer and metallic substrate and acting like oxidation barrier. The most used material for ceramic layer is yttria-stabilised zirconia (YSZ) due to its low thermal conductivity, relativity high thermal contraction coefficient and good mechanical properties at high temperature [2,3].

Atmospheric plasma spraying (APS) is an economical and versatile technique to obtain TBC. It consists on a plasma source where a feed material is melted and accelerated until it impacts upon substrate. On the substrate, molten (or partially molten) material is quickly cooled forming the coating [4]. In the last years, coatings from nanoparticles have been extensively addressed because different architectures as well as enhanced properties, compared with their convectional counterparts (from microstructured feedstocks) can be obtained. In the case of TBC, thermal conductivity can significantly be reduced and the thermal shock resistance can be ~~then~~ improved [5]. However, nanoparticles cannot be directly injected into the plasma plume due to their low specific weight and poor flowability. One possible solution for this problem is to reconstitute the nanoparticles into sprayable micrometric granules. The reconstitution process consists of spray drying of stable suspensions to obtain spherical free-flowing granules. Subsequently spray-dried powders are usually thermally treated in order to enhance the sinterability for the following, extremely fast sintering process in the plasma torch [6,7]. Coatings from reconstituted, nanostructured feedstocks usually display a bimodal

microstructure formed by partially melted agglomerates surrounded by fully melted particles which act as binder [6,7].

Although many research effort has been made to pass from the micro-scale to either the nano- or the submicron-scale using both powders or liquids as feedstock [8,9], few attempts have been made to use feedstocks comprising mixtures of different particle size distributions, e.g. submicron- and nano-sized particles. The use of a bimodal distribution of submicron-nano particles in the precursor suspension of the spray-dried powder can give rise to significant benefits during the suspension processing, i.e higher solids loading and lower viscosity leading to better properties in the resulting feedstock agglomerates, such as higher agglomerate bulk density and improved powder flowability [10,11]. However the relationship between these agglomerate feedstock characteristics and the final coating properties has been scarcely treated in the thermal spray literature despite the fact that this connection has been already proven in many other shaping processes [12-14]. Thus, some previous research was found in which the effect of agglomerate density and microstructure on TiO_2 coatings properties were addressed [15,16]. In addition some recent papers with YSZ systems have shown that agglomerate morphology and density can have an influence on coating microstructure and properties [17,18]. In this respect some of the authors of this paper have recently reported improved photocatalytic activity in APS TiO_2 coatings or enhanced mechanical properties in Al_2O_3-TiO_2 coatings when a mixture of nano- and submicron-sized particles in the spray-dried feedstock was used. Much higher density agglomerates were obtained which led to better properties in the final coatings [10,11]. These works reported that the microstructure and properties of plasma sprayed coatings not only depend on various process parameters but also are markedly influenced by the characteristics of the feedstock. Nevertheless this type of research trying to relate

feedstocks characteristics with coating microstructure and properties when nano- or submicron-structured feedstocks are used has not been addressed for YSZ coatings.

In a previous research the authors focused on the preparation of different YSZ spray-dried feedstocks starting from nano- and submicron-sized powders [19]. The paper aimed at obtaining suitable YSZ feedstocks for APS process including the starting suspension preparation and characterisation, spray-drying of suspensions, characterisation of spray-dried powders and their thermal treatment to complete the aforementioned reconstitution process. Finally, some of these powders were used to demonstrate that this methodology managed to produce feedstocks with adequate characteristics to be used in APS process. Most importantly the paper showed that the main feedstocks properties in terms of APS depositing process (agglomerate size and density as well as powder flowability) were very dependent of starting suspension characteristics.

Following this previous research this paper tries to close the loop by demonstrating the influence of feedstocks characteristics on the resulting APS coatings. Thus powders obtained from suspensions with different solid loadings and particle size distributions (nano- and submicron-sized mixtures) were deposited by APS onto stainless steel substrates. In addition two commercial (micro- and nano-structured) YSZ feedstocks were also deposited for comparison purposes. Then coatings were microstructurally and mechanically characterised. On the one hand, voids and partially melted areas were quantified by image analysis. On the other hand, microhardness and toughness were determined.

Experimental procedure

Feedstock preparation

The following commercial YSZ powders were used as raw materials: a nano-sized powder (5932HT, Nanostructured and Amorphous Materials Inc., USA) with a mean particle size of 40 nm and a specific surface area of 25.1 m^2/g; and a submicron-sized powder (TZ-3YS, Tosoh Co., Japan) with a mean particle size of 400 nm and a specific surface area of 6.8 m^2/g. Figure 1 shows the particle size distribution of these two powders obtained by dynamic light scattering (Zetasizer NanoZS, Malvern, UK) in the case of nanoparticles and laser diffraction (Mastersizer 200G, Malvern, UK) for submicron-sized particles. Both powders were made up of tetragonal phase while the nanopowder contained some minor (not quantified) monoclinic phase. On the other hand a commercial polyacrylic acid-based polyelectrolyte (DURAMAX^{TM} D-3005, Rohm & Haas/Dow Chemicals, USA) was used as dispersant for suspension preparation [12,20].

In the mentioned previous research the colloidal stability and rheological behaviour were evaluated to obtain stable and well-dispersed suspensions [19]. From this study, four aqueous YSZ suspensions with different solid loadings and different particle size distributions were selected. These suspensions were then reconstituted into sprayable granules by spray-drying (Mobile Minor, Gea Niro, Denmark) followed by thermal treatment. This treatment was carried out in an electric kiln with a soaking time of 60 min, at 1000 ºC for the powders obtained from nanoparticles (YnD and YnC), at 1200 ºC for the powder obtained from submicron-sized particles (YsC), and at 1050 ºC for the powder obtained from bimodal (nano- and submicron-sized) particle size

distribution (YsnC). These temperatures were chosen in the previous work with the aim of obtaining denser granules but at the same time of preserving as much as possible the nanostructure of the initial agglomerates [19]. Hence the spray dried powders were thermally treated at temperatures in which the sintering degree was only incipent (contraction value of around 1%).

Additionally two commercial YSZ feedstocks were used. One of them is a hollow-sphere (HOSP) micrometric powder (METCO 204NS, Sulzer-Metco, Germany) and the other one is a micrometric, nanostructured powder (Nanox S4007, Inframat Corp., USA). Hereafter these powders are referenced as YRm and YRn respectively. Further information and microgrphs of these two powders can be found elsewhere [21]. Due to the preparation routes followed to obtain these commercial powders YRm agglomerates were much more sintered than YRn agglomerates which were highly porous. All the feedstocks used in this work are described in table 1.

Feedstock characterisation

Feedstock powders were characterised before APS deposition. Field emission scanning electron microscope (FEG-SEM, S-4800, Hitachi, Japan) was used to analyse feedstock microstructure and the crystalline phases were determined by XRD (D8 Advance, Bruker AXS, Germany). Moreover, granule size distribution was measured by sieving. Granule apparent specific mass ($\rho_{granule}$) was calculated from tapped powder specific mass by assuming a theoretical packing factor of 0.6, which is characteristic of monosized, spherical particles [22]. Powder flowability was evaluated in terms of the Hausner ratio, which is the ratio of the tapped powder specific mass to the powder apparent specific mass. Free-flowing powders display a Hausner ratio below 1.25 [22]. Finally pore structure of feedstocks was assessed by mercury intrusion porosimetry, MIP (AutoPore IV 9500, Micromeritics, USA).

Coating deposition

YSZ coatings were deposited by an atmospheric plasma spray (APS) system. It consisted of a gun (F4-MB, Sulzer Metco, Germany) operated by an industrial robot (IRB 1400, ABB, Switzerland). Before spraying, the substrate was grit blasted with corundum at a pressure of 4.2 bars and cleaned with ethanol to remove any remaining dust or grease from the surface. A NiCrAlY bond coat was used to enhance the adhesion between the substrate and the ceramic layer. Deposition was performed using argon and hydrogen as plasma-forming gases. The same spraying conditions were used for all YSZ depositions: Ar flow=35 slpm, H_2 flow=12 slpm, arc intensity=600 A, spraying distance=0.1 m, spraying velocity=1 m/s (slpm: standard litre per minute). The necessary number of spraying passes was carried out to obtain a ceramic layer thickness of 150 μm.

Coating characterisation

First, coating microstructures were observed by FEG-SEM. Voids and partially melted areas of the coatings were evaluated by image analysis from 10 micrographs at 500x magnification. Averages values were then calculated.

Coatings were also mechanically characterised. The coating microhardness and fracture toughness were determined by microhardness tester (LECO M400, Leco Co., USA) performing 10 indentations for each coating to obtain an average value. 50 g indentation load was used to determine the microhardness while 1000 g indentation load was used for toughness assessment since a minimum load is required for the crack growth to occur. Niihara equation was used for toughness calculation [23].

Results and discussion

Feedstock characterisation

Morphology and structure of reconstituted powders (spray-dried+thermally treated) in this work are shown in figure 2. As it can be observed the powders contain spherical agglomerates displaying the typical doughnut-shape morphology of spray-dried agglomerates [24,25]. Most of granule sizes range from approximately 10 μm to 200 μm. The presence of some satellite-like granules stuck to bigger ones is also observed. Granules from diluted suspension of nanoparticles (YnD) seem to be smaller and their surface is quite rough due to the low viscosity of the starting suspension as set out in table 1. This finding coincides with that observed for nanoparticle suspensions of TiO_2 or Al_2O_3-TiO_2 mixtures obtained with different solids content [24,25]. On contrary the powder obtained from the high solids content suspension of nanoparticles (YnC) is made up of coarser granules containing large inner holes. This behaviour is due to the high viscosity of the starting suspension of this sample as indicated in table 1 [26]. On the other hand, higher magnification of the solid areas of the agglomerates of all the powders reveals that the granules are porous and formed by the agglomeration of the individual nano- and submicron-sized particles. On comparing nanostructured agglomerates (YnD and YnC) it can be observed that as the solid loading in the starting suspension rises the resulting agglomerates are denser [25]. Also when a bimodal mixture is used (YsnC versus YnC) i.e when submicron-sized particles are added to a nanoparticle suspension the resulting agglomerates are also denser due to enhanced particle packing effect [11]. Finally particle necking and coarsening is quite evident in all the samples as a consequence of the thermal treatment. As expected samples containing submicron-sized particles gave rise to coarser grains after the thermal treatment.

With regard to commercial powders, the characteristics of both samples have been reported elsewhere [21]. YRm powder consists of hollow spherical (HOSP) granules obtained by spray-drying and subsequent plasma-densifing process while YRn powder contains spherical, highly porous agglomerates formed by individual nanoparticles with diameters varying from approximately 30 to 130 nm.

Figure 3 shows the size distribution of the agglomerates comprising all the feedstocks. Although the curves represent sizes of thermal treated agglomerates it must be noticed that these sizes should practically coincide with those of the thermally untreated powders since the agglomerate shrinkage was, in all the samples, lower than 1% as mentioned above. As observed all the distributions display a monomodal pattern, significant differences among them appear though. The curves also confirm the micrometer size range of the spray-dried agglomerates. With regard to commercial samples, YRn nanostructured powder comprises agglomerates coarser than those of the reconstituted powders while granules of conventional YRm powder were slightly finer than those of the reconstituted powders. Among powders reconstituted in this work the graph shows that the higher the viscosity of the starting suspension (see table 1) the coarser the agglomerates confirming the aspect of the agglomerates displayed in the micrographs in figure 1. The correlation between starting suspension viscosity and agglomerate average size calculated from figure 3 data is plotted in figure 4. As it can be seen a good fit between both variables is obtained confirming the findings stated above.

To further characterise the agglomerate structure in all the samples mercury pore sizing was determined (figure 5). Although this technique determines any type of pore volume trapped in a powder bed, i.e. inter and intragranular porosity, in these curves only intragranular porosity is displayed owing to the scarce interest of the porosity trapped

between agglomerates when the performance of the agglomerates inside the plasma torch in an APS process is to be analysed. Focusing on the reconstituted powders, YnD and YnC display a very similar intragranular porosity. However when submicron-sized particles are mixed with nanoparticles (sample YsnC) the resulting agglomerates are slightly less porous but more importantly display larger pore sizes as a consequence of the increased particle size inside the agglomerates. This same trend is observed when the amount of submicron-sized particles is increased up to 100% (YsC sample). These findings show that granule porosity and pore size basically depends on the particle size distribution of the solids comprising the agglomerates. Thus the wider particle size distribution of the submicron-sized powder (see figure 1) when compared with the distribution of the nanosized powder results in denser particle packing inside the agglomerate. These findings agree with theoretical models on particle packing of continuous particle size distributions [27]. YsnC sample porosity lies between YnC and YsC porosity values. Regarding commercial samples, low porosity in YRm powder curve relates to the HOSP nature of this feedstock (the large inner hole of the HOSP granule is not considered in the pore sizing curve) while YRn sample exhibits its high porosity agglomerate characteristic.

Figure 6 shows Hausner ratio and agglomerate apparent specific mass of the feedstocks. All powders present a Hausner ratio lower than 1.25 therefore they display a free-flowing nature. Even though little differences on flowability were observed among the different feedstocks, YnD sample shows the worst flowability (the highest Hausner ratio) as a consequence of a combined effect of small agglomerate size and high surface roughness. Regarding granule apparent specific mass, significant differences were found between the reconstituted powders as expected from the pore sizing assessment. To better visualise these differences, figure 7 plots the variation of agglomerate

apparent specific mass of the four reconstituted powders versus the amount of submicron-sized particles in the starting suspension. As it can be observed, a clear, linear relationship between both variables has been found confirming the findings observed in the porosimetry analysis. The higher the amount of submicron-sized particles in the starting suspension the higher the agglomerate density is. Figure 8 confirms the good agreement between the values of agglomerate apparent specific mass calculated from the powder tapped specific mass as set out above and those obtained from mercury pore sizing curves (figure 5). In respect of commercial feedstocks as expected agglomerate apparent specific mass of YRm (HOSP) agglomerate is much higher than that of the YRn agglomerate. Finally it is important to note that all the powders met the recommendations to be deposited by APS (Hausner ratio lower than 1.25, granule apparent specific mass higher than 1700 kg /m^3 and mean granule size higher than 20 μm) [4,7].

Coating microstructure

Commercial and reconstituted feedstocks were deposited by APS. Figure 9 shows the cross-section microstructure of the resultant coatings. As observed all the coatings were porous, exhibiting the typical lamellar structure of plasma sprayed coatings. This microstructure comprises smaller pores located within individual lamellae and larger pores trapped along the interlamellar boundaries. Figure 9 also reveals that coatings microstructure is influenced by the feedstock characteristics. Hence layers deposited from the nanostructured feedstocks (YnD and YnC) exhibit a bimodal microstructure formed by partially melted agglomerates (marked PM in the micrographs) that retain some of the initial nanostructure, surrounded by a fully melted matrix (marked M in the micrographs). Such microstructure has been extensively reported in literature [6-8] in

which details on the features of these partially-melted areas can be found. Thus despite the nanostructured character of the primary particles comprising the feedstock, the relatively high porosity associated to these agglomerates results in coatings containing partially melted areas which preserve in some extent the starting nanostructure. This statement is particularly evident in the commercial, nanostructured powder which showed the highest agglomerate porosity (figure 5) giving rise to much higher amount of partially-melted areas as observed in the corresponding micrograph of figure 9. Respecting coatings obtained from submicron-sized particles (YsnC and YsC feedstocks) higher amount of partially-melted areas when compared with coatings obtained from nanostructured feedstocks (YnD and YnC) are observed. These findings seem to indicate that for similar values of agglomerate porosity feedstocks containing coarser particles (submicron-sized) lead to higher amount of partially-melted areas in the coatings provided that energy conditions during the plasma spray are also similar. These findings have been previously observed during deposition by APS of nano- and submicron-sized titania particles [11]. The different features of these partially-melted zones can be observed in figure 10. As expected nanoparticles were retained in the partially melted zones of YnD and YnC coatings but some of them were partially sintered so that micrometric voids and coarser grains were also found. On the other hand partially melted zones of YsC coatings exhibit the initial agglomerate microstructure. Finally, coating obtained from the commercial, microstructured powder (YRm sample) presents a quite homogeneous microstructure containing low amount of partially-melted areas what agrees with the highly sintered microstructure of the HOSP agglomerates.

In view of the above, the total porosity of the coatings as well as the amount of partially-melted areas were estimated by image analysis at 500 magnifications from

SEM pictures following a procedure set out elsewhere [11,25]. Figure 11 shows the porosity and partially-melted areas values obtained for all the coatings. Porosity data agree with the typical values observed in these types of coatings. Besides, in all the coatings reconstituted in this work the porosity values were very similar. This is because, at this low range of coating porosities the contribution of the agglomerate density to the final coating porosity is negligible as compared with the contribution coming from the melting and subsequent deformation of the agglomerates during the deposition process. On contrary larger differences among the coatings were observed for the values of the partially-melted areas content. Coatings obtained from feedstocks containing submicron-sized particles (YsC and YnsC) display higher amount of partially-melted areas in comparison with the feedstocks exclusively formed by nanoparticles (YnD and YnC). Thus for a given plasma spray conditions (plasma energy) the amount and the size of the particles inside these partially-melted zones obviously depend on the size of the particles comprising the feedstock agglomerates (nanoparticles or submicron- sized particles) but also on other feedstock characteristics such as agglomerate size and density. As the agglomerate size and porosity of the reconstituted feedstocks are not so different the findings obtained highlight the role of the particle size in reconstituted, spray-drying agglomerated powders with regard to the appearance of the always existing partially-melted areas. Finally, the quantified amount of partially-melted areas for the coatings obtained from the commercial feedstocks (YRm and YRn) agrees well with the appreciation deduced from the corresponding micrographs in figure 9.

Coating properties

Figure 12 displays microhardness and toughness of the coatings obtained from the different feedstocks. Coatings from commercial powders exhibit lower values of microhardness, in particular YRn coating which presented the highest value of porosity as set out above. Thus the negative effect of porosity on microhardness can easily be noted in this coating in which the porosity value almost doubles those of the rest of coatings. This effect has been extensively reported in APS literature [28,29]. In less extent, the effect of porosity can be also observed in the other commercial coating (YRm) which also shows lower microhardness due to its relatively high porosity. As regards the coatings obtained from the reconstituted feedstocks, higher values of microhardness were found on comparing with the coatings obtained from the commercial feedstocks owing to their lower porosity values. Nevertheless no clear relationship between porosity and microhardness were observed for this group of coatings. This is because differences in porosity were too small for the correlation to be established (see figure 11). On the other hand literature on coatings obtained from nanostructured feedstocks reports that the presence of mechanically weak partially-molten zones featuring these coatings can result in mechanical properties decrease [30]. Hence, although this effect can contribute to the low hardness of YRn coating, it has not been observed in the case of YsC and YsnC coatings despite the fact that these coatings contained higher amount of partially-melted areas than YnD and YnC coatings. This discrepancy with the reported data can be caused by the higher density of the partially-melted areas in coatings which have been obtained from feedstocks containing submicron-sized particles (YsC and YsnC coatings) as observed in figure 10.

Finally, according to literature, partially melted zones present in coatings obtained from nanostructured feedstocks can behave as barriers for crack propagation [5,7]. However

few changes in terms of toughness were found between conventional coating (YRm) and coatings from nanostructured feedstocks (YnC, YnD and ~~YRc).~~ It is probably because of the poor cohesion presented by the partially melted zones of these coatings. On contrary, the higher toughness value for YsC coating can be attributed to its larger amount of denser partially molten zones as set out above.

Conclusions

In this work, YSZ coatings were obtained from different feedstocks by APS. On the one hand four reconstituted powders from nano- and submicron-sized particles were deposited. The reconstitution process consisted in spray-drying of the starting suspension followed by a thermal treatment of the spray-dried agglomerates. In addition, two commercial powders (one nanostructured and the other one conventional) were also deposited to compare differences between the final coatings. It was proven that suspension characteristics strongly affect the spray-dried agglomerate properties. Thus the higher the suspension viscosity the coarser the spray-dry agglomerate size whereas the agglomerate density is directly related to the amount of submicron-sized particles in the starting suspension. All the reconstituted feedstocks showed adequate properties to be used in an APS process.

The coatings obtained displayed a bimodal microstructure formed by partially melted zones surrounded by a fully melted matrix. Coating porosity and the amount of partially melted areas depend on the feedstock characteristics. As the coating microstructure (porosity and amount of partially melted areas) strongly defines the mechanical properties of the final coatings this work has proven the connection between the mechanical properties of the coatings and the characteristics of the feedstock

agglomerates. On the one hand, coatings obtained from the reconstituted feedstocks gave rise to higher values of microhardness when compared with the coatings obtained from the commercial feedstocks owing to the lower porosity of the reconstituted powders. On the other hand, the effect of the characteristics of the partially melted areas on microhardness has been also put forward. Nevertheless the effect of these partially-melted areas on microhardness is not so impacting as that of coating porosity. Finally the reinforcing role of the amount of partially-melted areas on the coating toughness as reported in the literature has not been observed in this work. In fact no differences in toughness were found between the conventional coating which did not contain any partially-melted areas and the coatings obtained from reconstituted feedstocks which presented different amounts of these areas.

Acknowledgments

This work has been supported by the Spanish Ministry of Science and Innovation (project MAT2012-38364-C03), by the Research Promotion Plan of the Universitat Jaume I, action 3.1 (ref. PREDOC/2009/10) and it has been co-funded by ERDF (European Regional Development Funds). The authors also acknowledge the SCIC of Valencia University for the FEG-SEM observations. Finally the Spanish Ministry of Science and Innovation for Juan de la Cierva contract (JCI-2011-10498) is also grateful.

Reference

1. R. Vassen, A. Stuke, D. Stöver, Recent developments in the field of thermal barrier coatings, Therm. Spray Technol. 18 (2009) 181-186.
2. D.R. Clarke, S.R. Phillpot, Thermal barrier coatings materials, Mater. Today 8 (2005) 22-29.

3. N.P. Patdure, M. Gell, E.H. Jordan, Thermal barrier coatings for gas-turbine engine applications, Science 296 (2002) 280-284.
4. P. Fauchais, G. Montavon, G. Bertrand, From powders to thermally sprayed coatings, Therm Spray Technol 18 (2009) 56-80.
5. R.S. Lima, B.R. Marple, Thermal spray coatings engineered from nanostructured ceramic agglomerated powders for structural, thermal barrier and biomedical applications: A review, Therm Spray Technol 16 (2007) 40-63.
6. L. Pawlowski, Finely grained nanometric and submicrometric coatings by thermal spraying: A review, Surf. Coat. Technol. 205 (2008) 4318-4328.
7. P. Fauchais, G. Montavon, R.S. Lima, B.R. Marple, Engineering a new class of thermal spray nano-based microstructures from agglomerated nanostructured particles, suspensions and solutions: an invited review, J. Phys. D: Appl. Phys., 2011, 44 (9) 93001.
8. B.R. Marple, R.S. Lima, Engineering nanostructured thermal spray coatings: process-property-performance relationships of ceramic based materials, Adv. Appl. Ceram. 106 (2007) 265-275.
9. D. Waldbillig, O. Kesler, The effect of solids and dispersant loadings on the suspension viscosities and deposition rates of suspension plasma sprayed YSZ coatings, Surf. Coat. Technol. 203 (2009) 2098-2101.
10. M. Vicent, E. Bannier, R. Moreno, M.D. Salvador, E. Sánchez, Atmospheric plasma spraying coatings from alumina-titania feedstock comprising bimodal particle size distribution, J. Eur. Ceram. Soc. 33 (2013) 3313-3324.
11. M.C. Bordes, M. Vicent, A. Moreno, R. Moreno, A. Borrell, M.D. Salvador, E. Sánchez, Microstructure and photocatalytic activity of APS coatings obtained from different TiO_2 nanopowders, Surf. Coat. Technol. 220 (2013) 179-186.

12. R. Benavente, M.D. Salvador, M.C. Alcázar, R. Moreno, Dense nanostructured zirconia compacts obtained by colloidal filtration of binary mixtures, Ceram. Int. 38 (2010) 2111-2117.
13. T. Molina, M. Vicent, E. Sánchez, R. Moreno, Stability and EPD concentrated suspensions of alumina with nanosized titania, Key Eng. Mater. 507 (2012) 203-207.
14. I. Santacruz, M.I. Nieto, J. Binner, R. Moreno. Wet forming of concentrated nano $BaTiO_3$ suspensions. J. Eur. Ceram. Soc. 29 (2009) 881-886.
15. G. Bertrand, N. Berger-Keller, C. Meunier, C. Coddet, Evaluation of metastable phase and microhardness on plasma sprayed titania coatings, Surf. Coat. Technol. 200 (2006) 5013-5019.
16. N. Berger-Keller, G. Bertrand, C. Filiare, C. Meunier, C. Coddet, Microsctructure of plasma-sprayed titania coatings deposited from spray-dried powder, Surf. Coat. Technol. 168 (2003) 281-290.
17. M.R. Loghman-Estarki, H. Edris, R.S. Razavi, R. Ghasemi, M. Pourbafrany, M. Ramezani, Spray drying of nanometric SYSZ powders to obtain plasma sprayable nanostructured granules, Ceram. Int. 39 (2013) 9447-9457.
18. M.R. Loghman-Estarki, M. Pourbafrany, R.S. Razavi, H. Edris, S.R. Bakhshi, M. Erfanmanesh, H. Jamali, S. N.Hosseini, M.Hajizadeh-Oghaz, Preparation of nanostructured YSZ granules by the spray-drying method, Ceram. Int. 40 (2014) 3721-3729.
19. P. Carpio, R. Moreno, A. Gómez, M.D. Salvador, E. Sánchez, Role of suspension preparation in the reconstitution process to obtain nano/submicrostructured YSZ powders for atmospheric plasma spraying, J. Eur. Ceram. Soc. Accepted

20. S. Fazio, J. Guzmán, M.T. Colomer, A. Salomoni, R. Moreno. Colloidal stability of nanosized titania aqueous suspensions, J. Eur. Ceram. Soc. 28 (2008) 2171-2176.
21. R.S. Lima, B.R. Marple, Nanostructured YSZ thermal barrier coatings engineered to counteract sintering effects, Mater. Sci. Eng. A, 485 (2008) 182-193.
22. J.L. Amorós, A. Blasco, J.E. Enrique, F. Negre, Características de polvos cerámicos para prensado [~~Characteisitics~~ of ceramic powders for pressing], Bol. Soc. Esp. Ceram. Vidr. 79 (1987) 3033-3040.
23. K. Niihara, R. Morena, D.P.H. Hasselman, Evaluation of K_{IC} of brittle solids by the indentation method with low crack-to-indent ratios, J. Mat. Sci. Lett. 1 (1982) 13-16.
24. M. Vicent, E. Sánchez, A. Moreno, R. Moreno, Preparation of high solids content nano-titania suspensions to obtain spray-dried nanostructured powders for atmospheric plasma spraying, J. Eur. Ceram. Soc. 31 (2012) 185-194.
25. E. Sánchez, A. Moreno, M. Vicent, M.D. Salvador, V. Bonache, E. Klyatskina, I. Santacruz, R. Moreno. Preparation and spray drying of Al_2O_3-TiO_2 nanoparticle suspensions to obtain nanostructured coatings by APS, Surf. Coat. Technol. 208 (2010) 987-992.
26. K. Masters, Spray drying handbook, fifth ed., Longman Scientific & Technical, Harlow, 1991.
27. J.S. Reed, Principles of ceramic processing, second ed., John Wiley, New York, 1995.
28. S. Karthikeyan, V. Balasubramanian, R. Rajendran, Developing empirical relationships to estimate porosity and microhardness of plasma-sprayed YSZ coatings, Ceram. Int. 40 (2014) 3171–3183.

29. M. Alfano, G. Di Girolamo, L. Pagnota, D. Sun, J. Zekonyte, R.J.K. Wood, The influence of high-temperature sintering on microstructure and mechanical properties of free-standing APS CeO_2-Y_2O_3-ZrO_2 coatings, J. Mater. Sci. 45 (2010) 2622-2669.

30. L. Wang, Y. Wang, X.G. Sun, J.Q. He, Z.Y. Pan, C.H. Wang, Microstructure and indentation mechanical properties of plasma sprayed nano-bimodal and convencional ZrO_2-8wt%Y_2O_3 thermal barrier coatings, Vacuum 86 (2012) 1174-1185.

Figure captions

Figure 1. Particle size distribution of the commercial nano- (n) and submicron-sized (s) particles

Figure 2. FEG-SEM micrographs at different magnifications of reconstituted feedstocks (thermally treated spray-dried powders): a) YnD; b) YnC; c) YsC; d) YsnC

Figure 3. Agglomerate size distributions of the feedstocks

Figure 4. Correlation between starting suspension viscosity displayed in table 1 and agglomerate average size worked out from figure 3

Figure 5. Pore size distribution of the feedstocks obtained by mercury intrusion porosimetry. Only intragranular porosity is taken into account

Figure 6. Hausner ratio and agglomerate apparent specific mass ($\rho_{agglomerate}$) of the feedstocks

Figure 7. Variation of agglomerate apparent specific mass ($\rho_{agglomerate}$) versus the amount of submicron-sized particles in the starting suspension

Figure 8. Relation between agglomerate apparent specific mass of the six powder feedstocks as obtained from the powder tapped specific mass and mercury pore sizing procedures

Figure 9. Coating cross section micrographs at 500x magnification. Melted and partially-melted areas are referenced as M and PM respectively

Figure 10. Partially melted zone detail of different coatings

Figure 11. Porosity and partially melted areas of the coatings as determined by SEM

Figure 12. Microhardness and toughness of the different coatings

Table caption

Table 1. Reference and description of all the YSZ feedstocks used through this work

Reference	Starting suspension			$T_{treatment}$ [3] (ºC)
	Solids	SL [1] (vol.%)	μ [2] (mPa·s)	
YnD	100% nanoparticle	10	2.8	1000
YnC	100% nanoparticle	30	46.5	1000
YsC	100% submicron-sized particle	30	13.3	1200
YsnC	50% nano- + 50% submicron-sized particle	30	17.9	1150
YRm	Commercial (reference) microstructured powder			
YRn	Commercial (reference) nanostructured powder			

[1] SL: solid loading

[2] μ: suspension viscosity measured from downward flow curves at shear rate of 1000 s^{-1} (reference 19).

[3] $T_{treatment}$: temperature of the powder thermal treatment (reference 19).

Figure 1

Click here to download high resolution image

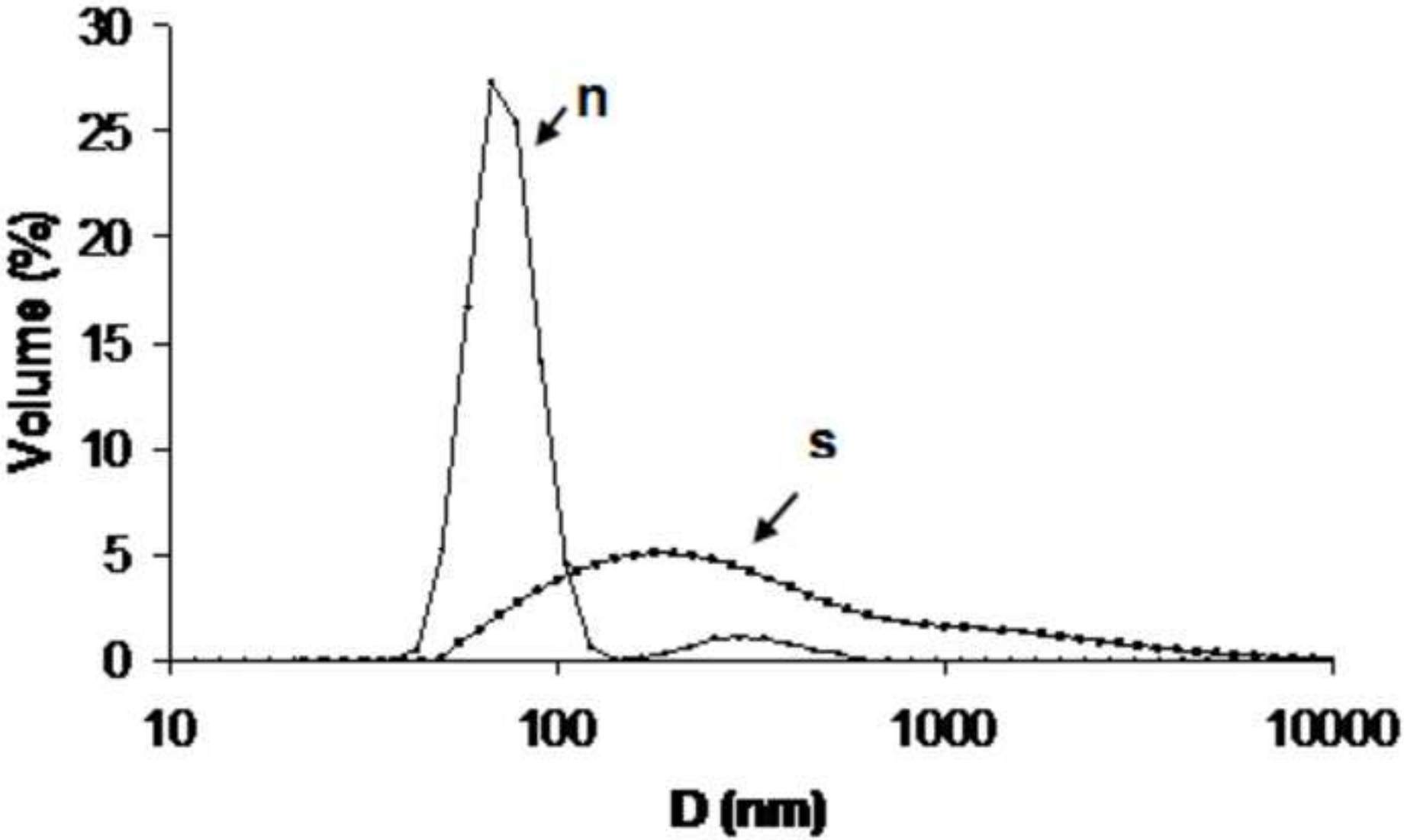

Figure 2

Click here to download high resolution image

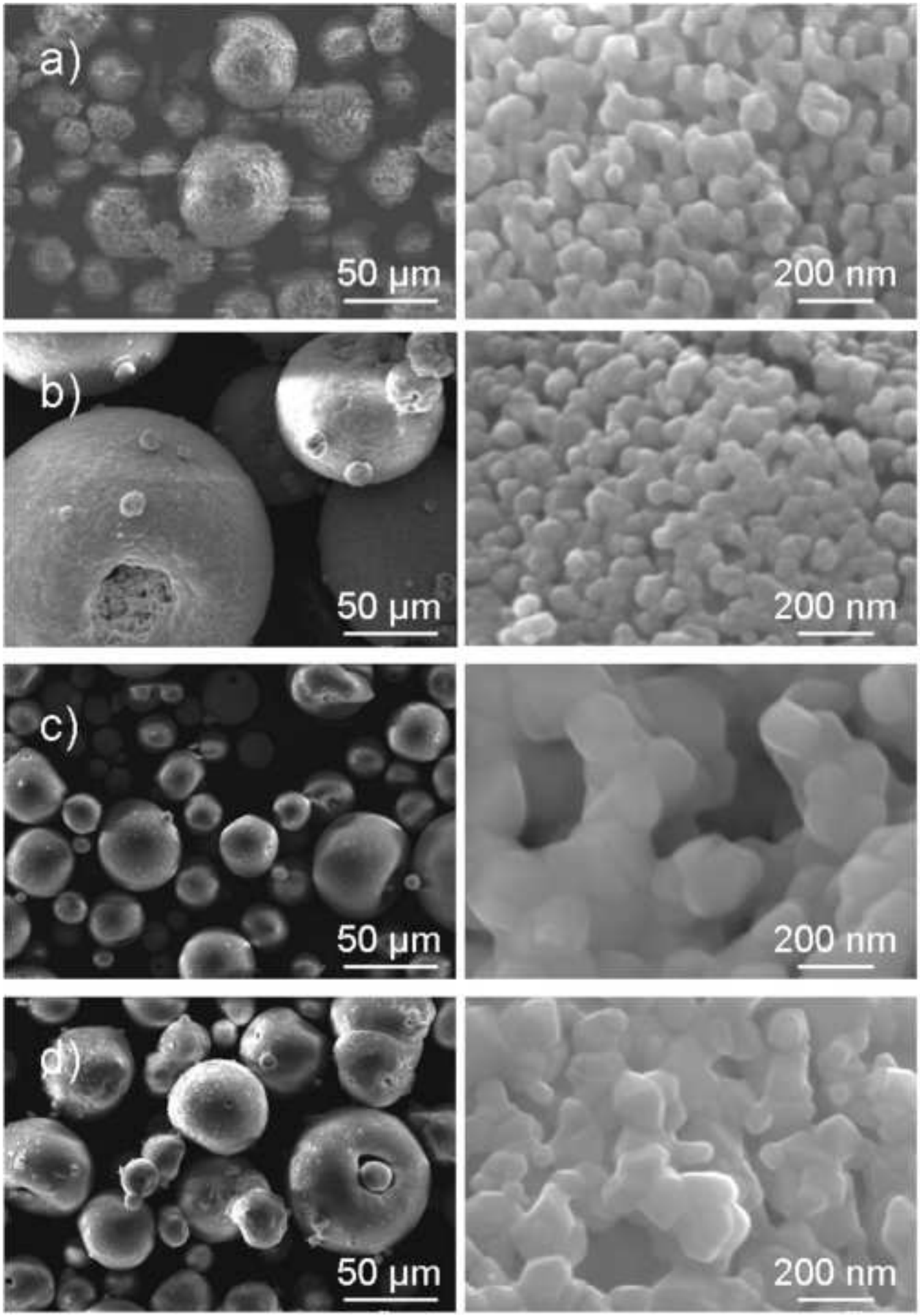

Figure 3

Click here to download high resolution image

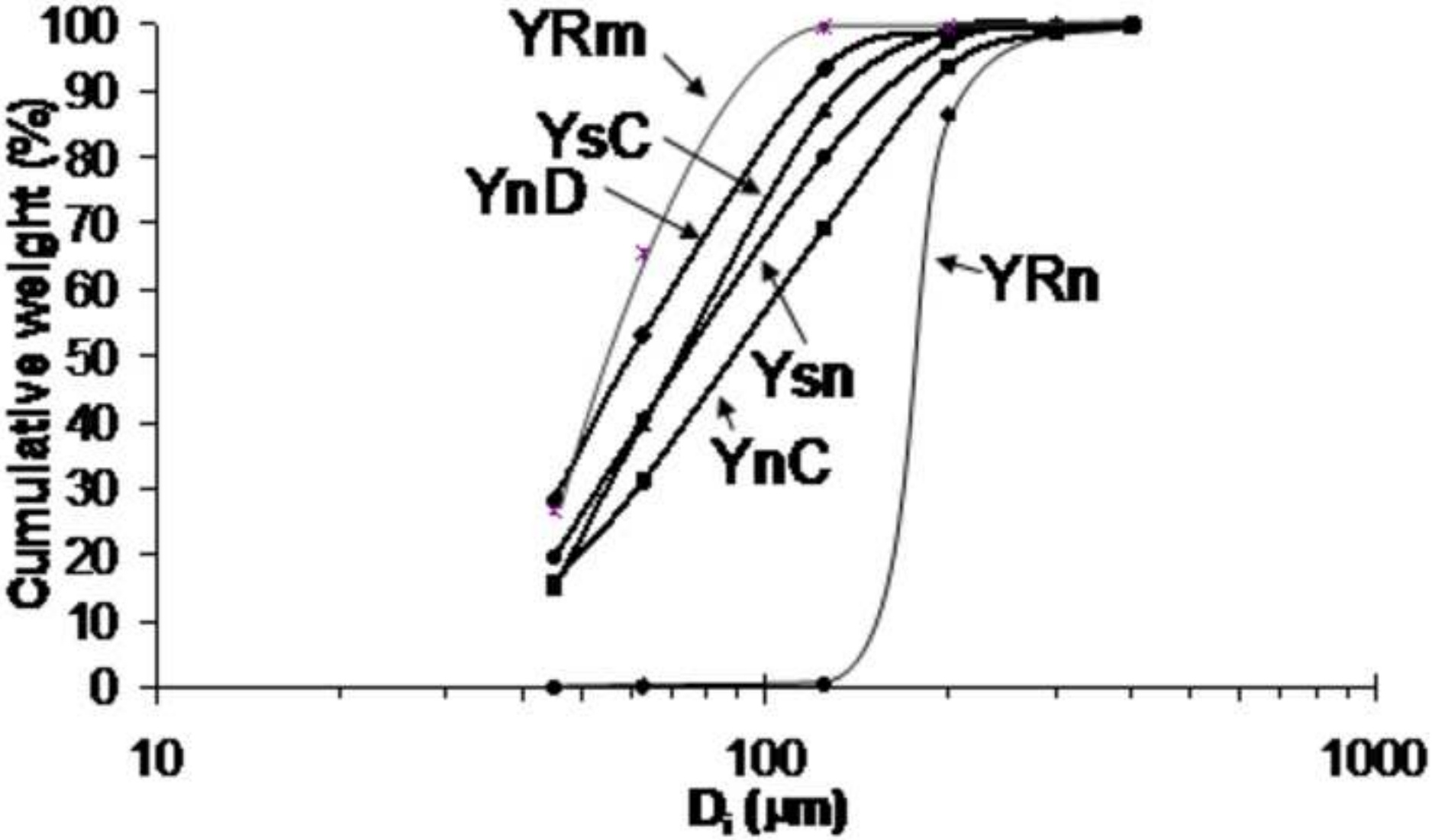

Figure 4

Click here to download high resolution image

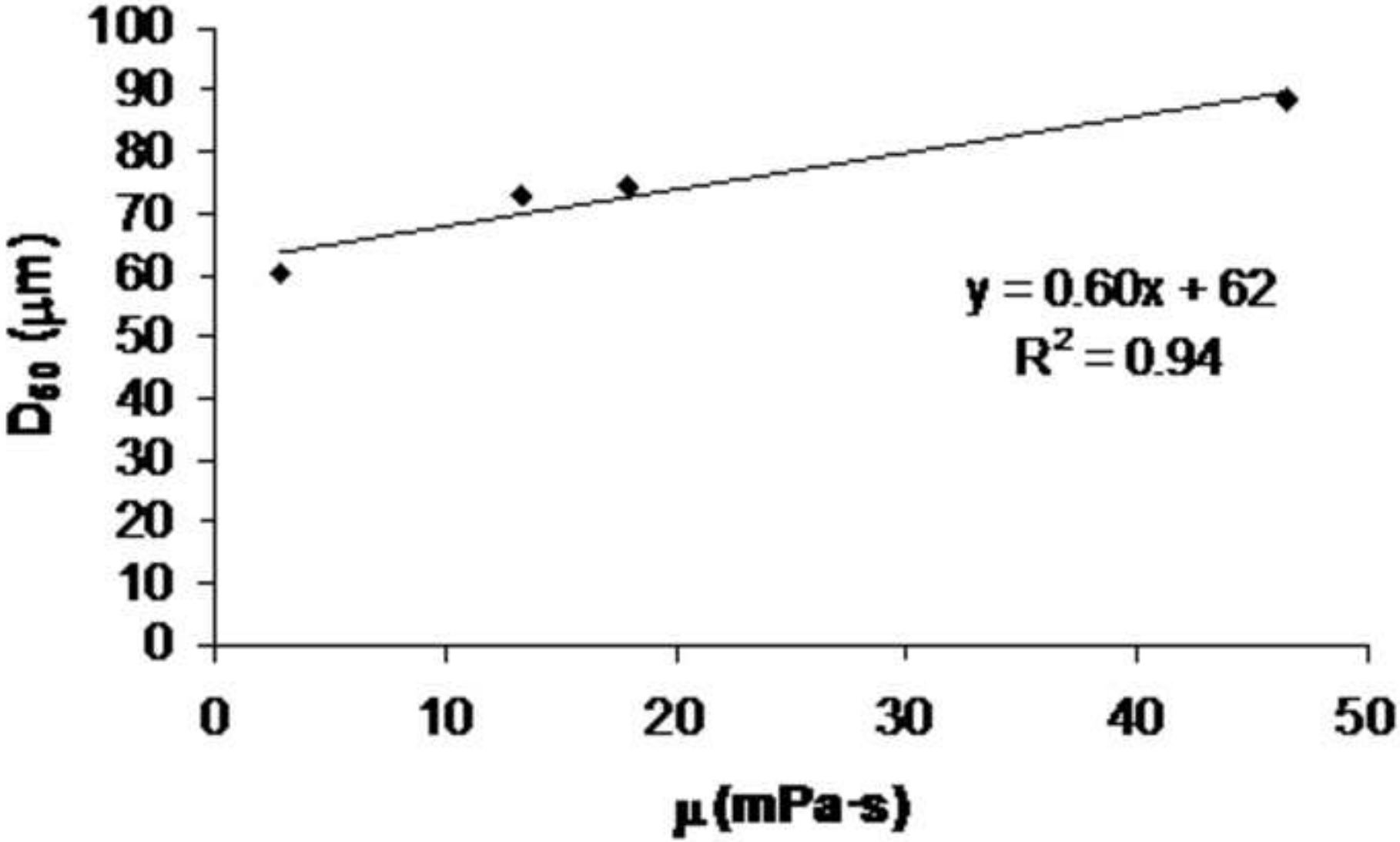

Figure 5

Click here to download high resolution image

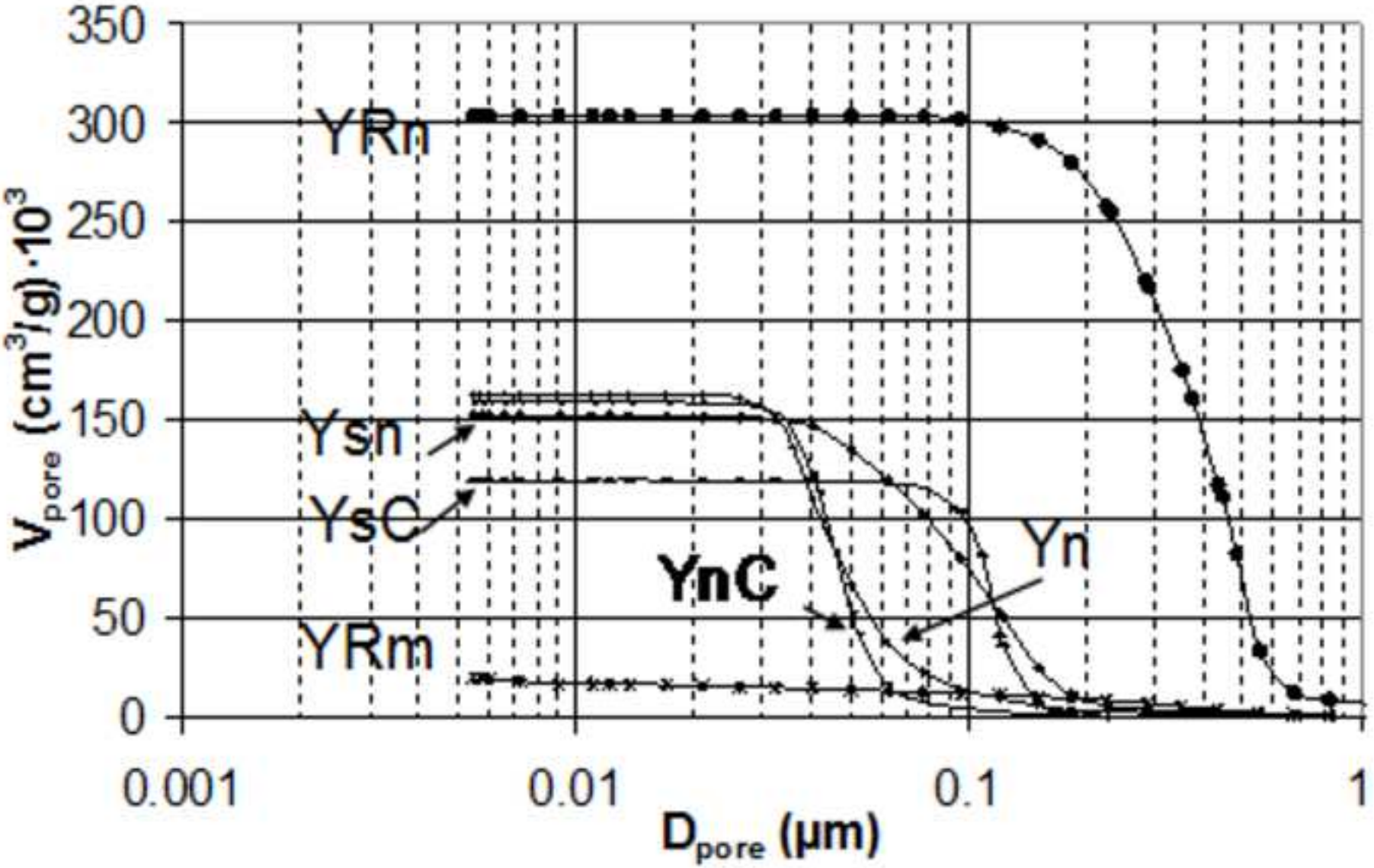

Figure 6

Click here to download high resolution image

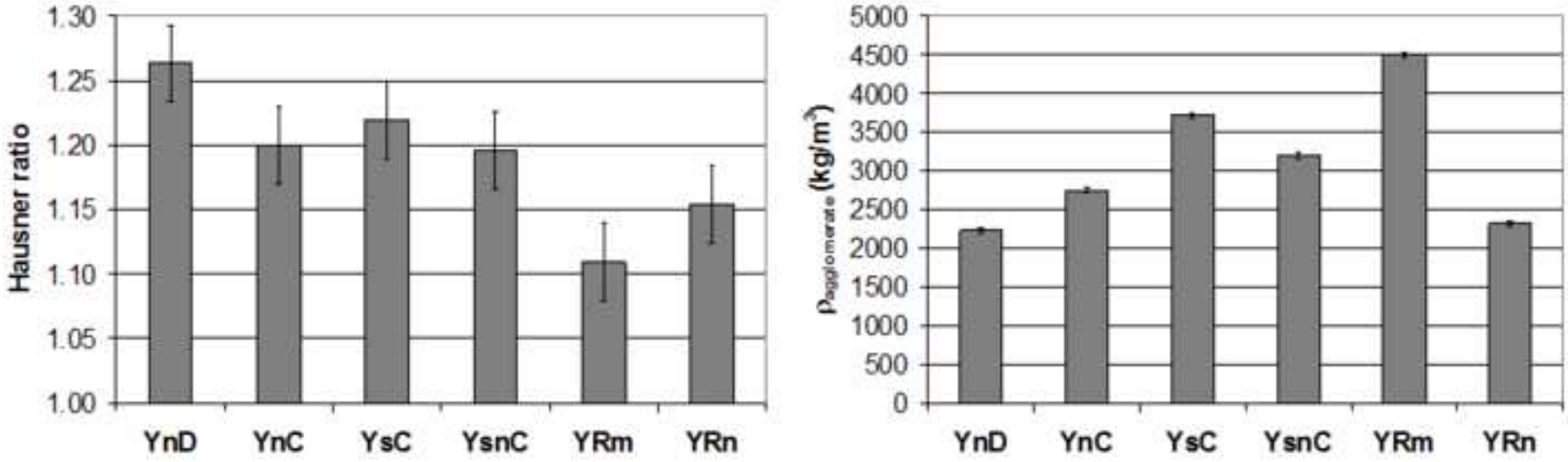

Figure 7

Click here to download high resolution image

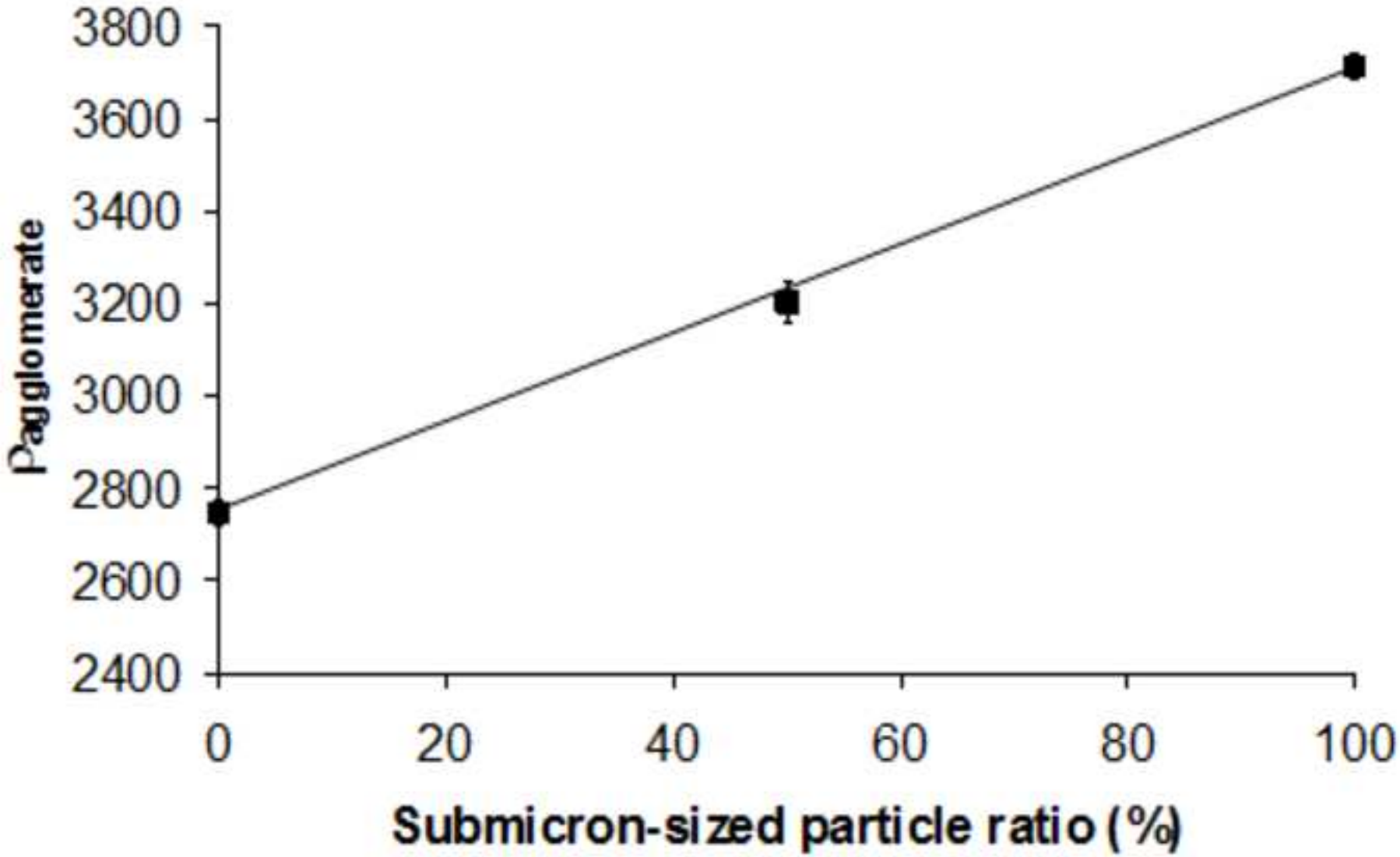

Figure 8

Click here to download high resolution image

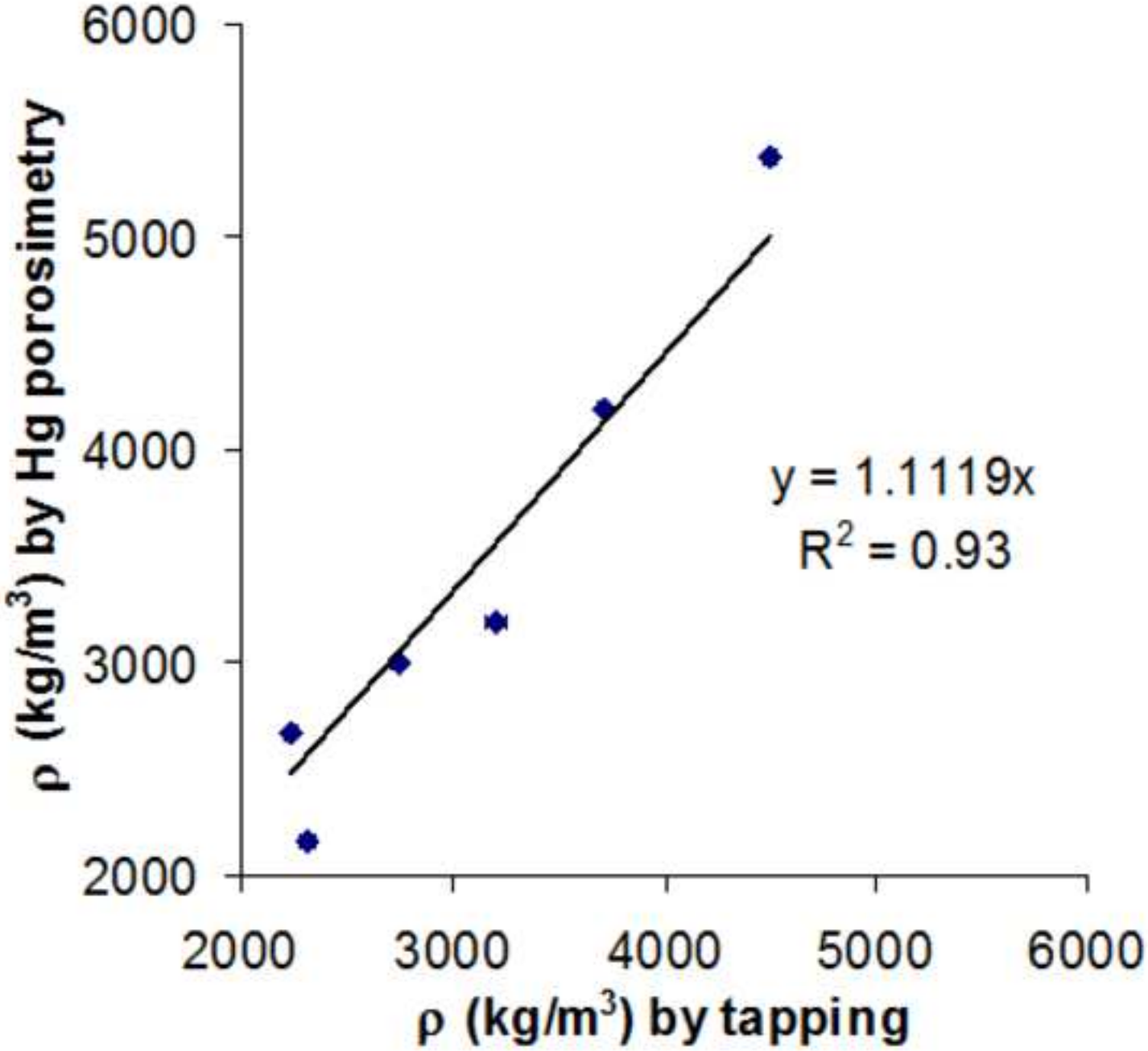

Figure 9
Click here to download high resolution image

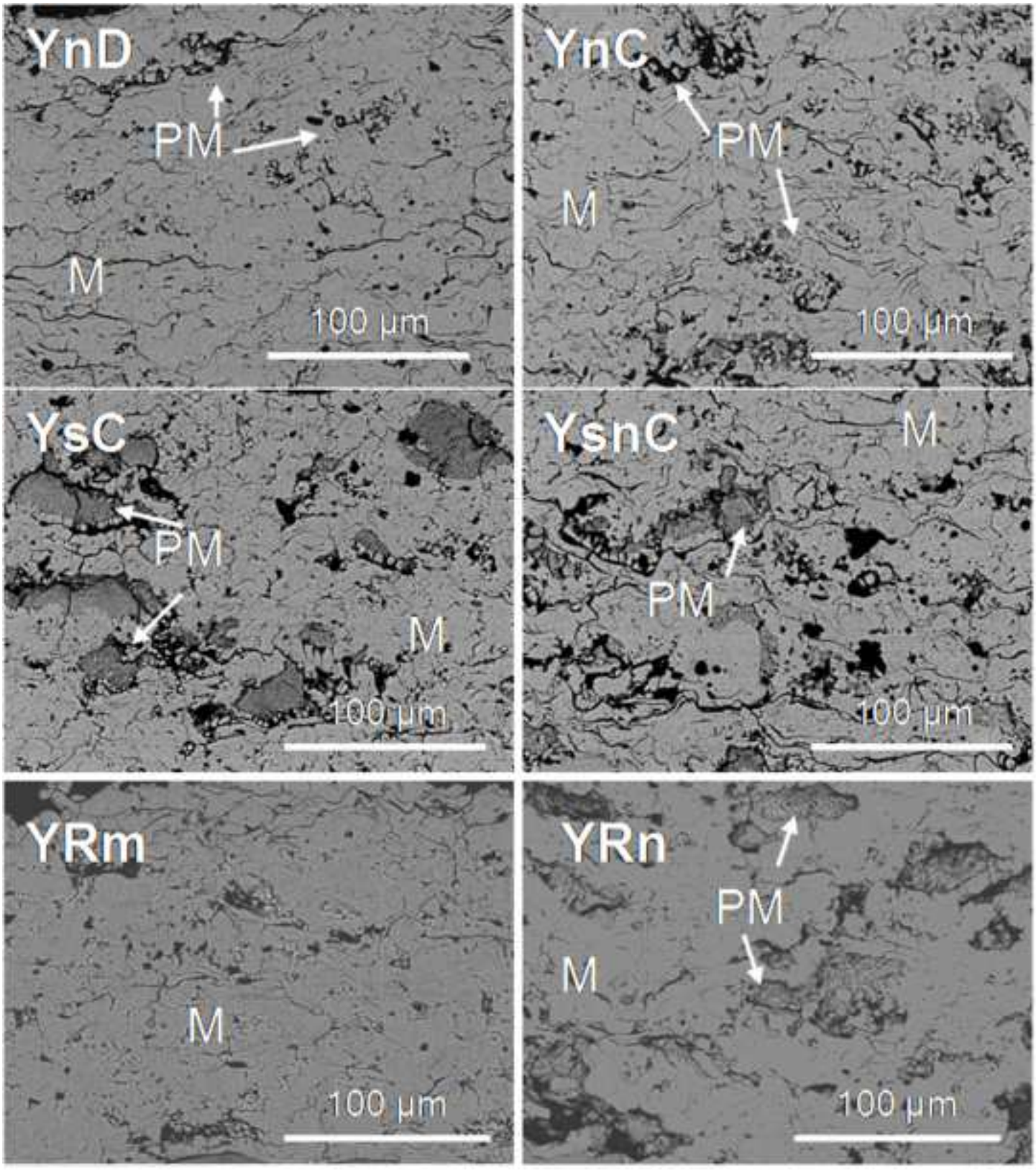

Figure 10

Click here to download high resolution image

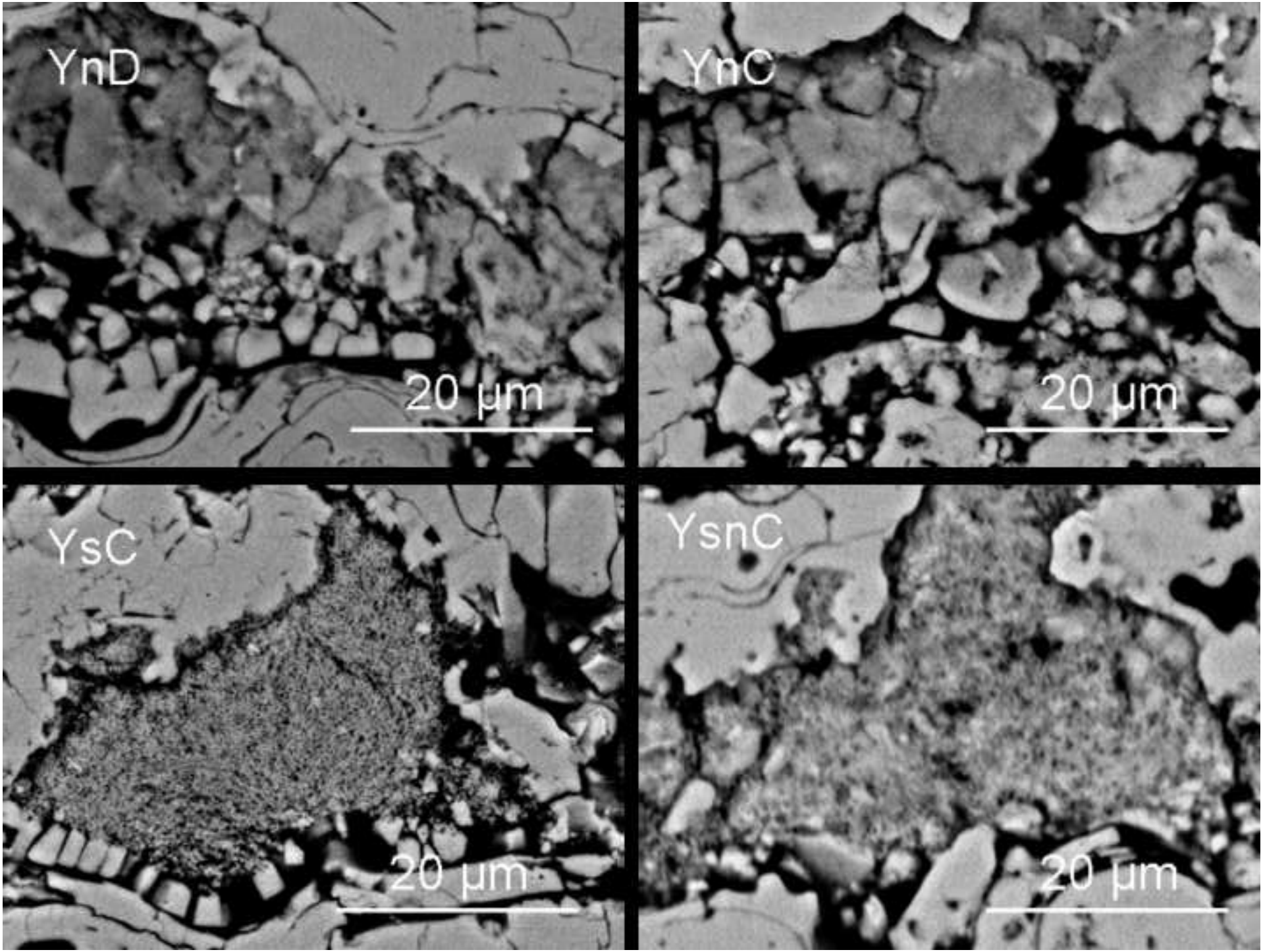

Figure 11

Click here to download high resolution image

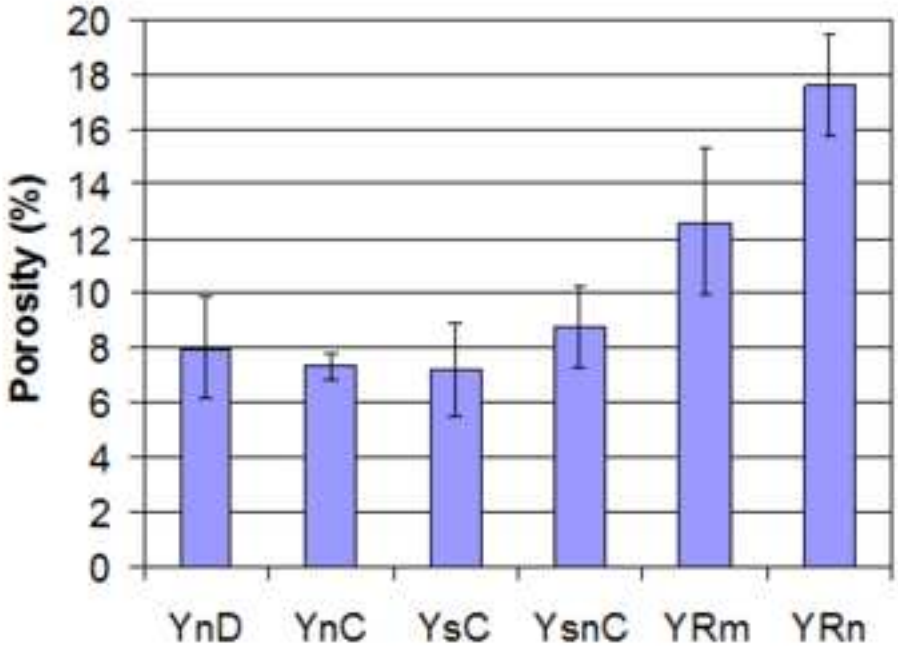

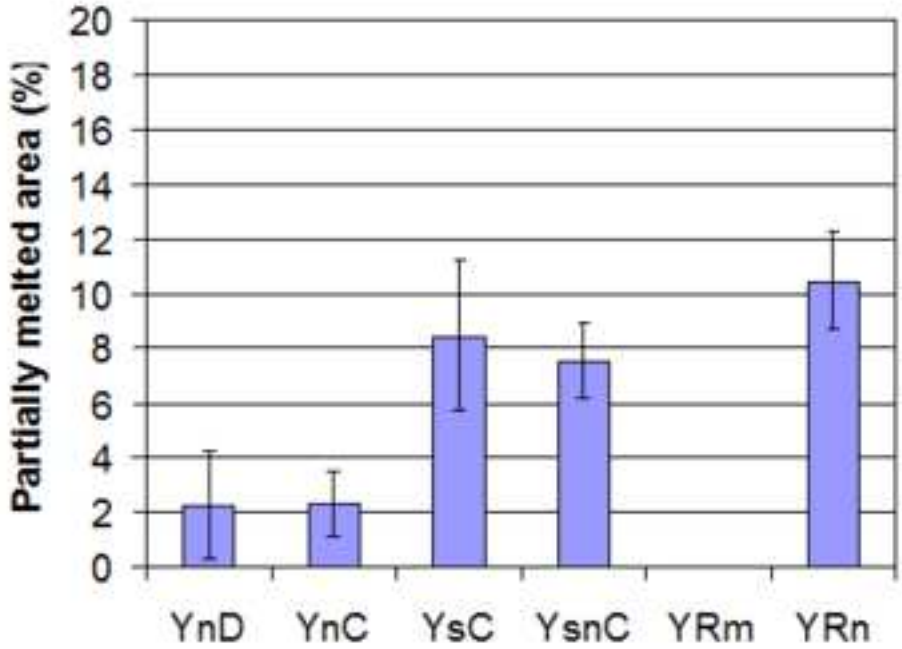

Figure 12

Click here to download high resolution image